Archives of Biochemistry and Biophysics 674 (2019) 108114

Contents lists available at ScienceDirect

Archives of Biochemistry and Biophysics

journal homepage: www.elsevier.com/locate/yabbi

Effect of oxidative stress on cystine transportation by xC^- antiporter

Maryam Ghasemitarei[a,b,*], Maksudbek Yusupov[b], Jamoliddin Razzokov[b], Babak Shokri[a], Annemie Bogaerts[b]

[a] Physics Department, Shahid Beheshti University, G.C., Evin, Tehran, 19839, Iran
[b] Research Group PLASMANT, Department of Chemistry, University of Antwerp, Universiteitsplein 1, B-2610, Antwerp, Belgium

A B S T R A C T

We performed computer simulations to investigate the effect of oxidation on the extracellular cystine (CYC) uptake by the xC^- antiporter. The latter is important for killing of cancer cells. Specifically, applying molecular dynamics (MD) simulations we studied the transport of CYC across xCT, i.e., the light subunit of the xC^- antiporter, in charge of bidirectional transport of CYC and glutamate. We considered the outward facing (OF) configuration of xCT, and to study the effect of oxidation, we modified the Cys_{327} residue, located in the vicinity of the extracellular milieu, to cysteic acid (CYO_{327}).

Our computational results showed that oxidation of Cys_{327} results in a free energy barrier for CYC translocation, thereby blocking the access of CYC to the substrate binding site of the OF system. The formation of the energy barrier was found to be due to the conformational changes in the channel. Analysis of the MD trajectories revealed that the reorganization of the side chains of the Tyr_{244} and CYO_{327} residues play a critical role in the OF channel blocking. Indeed, the calculated distance between Tyr_{244} and either Cys_{327} or CYO_{327} showed a narrowing of the channel after oxidation. The obtained free energy barrier for CYC translocation was found to be 33.9kJmol^{-1}, indicating that oxidation of Cys_{327}, by e.g., cold atmospheric plasma, is more effective in inhibiting the xC^- antiporter than in the mutation of this amino acid to Ala (yielding a barrier of 32.4kJmol^{-1}). The inhibition of the xC^- antiporter may lead to Cys starvation in some cancer cells, eventually resulting in cancer cell death.

1. Introduction

In recent years, cold atmospheric plasma (CAP) is frequently applied in biology and medicine [1]. Fields of application include the treatment of dental cavities [2], sterilization of various surfaces [3], cancer treatment [4], and wound healing [5]. Particularly, in the last decade, CAP has shown considerable anti-cancer capacity for various types of cancer cells [6]. CAP (or simply plasma) can selectively treat cancer cells, without (seriously) damaging normal cells [7–9], and up to now, cancer cells have not yet developed resistance against plasma treatment [10–13]. The generally accepted theory about the anti-cancer ability of plasma is based on oxidative stress [14]. The reactive oxygen species (ROS) formed in plasma, which can also be generated by some other traditional anti-cancer therapies, are believed to be responsible for apoptosis in cancer cells. The different cell cycle of healthy and cancer cells [15], the higher concentration of ROS and RNS (i.e., reactive nitrogen species) found in cancer cells [16], the higher expression of aquaporin channels in cancer cell membranes [17,18], and the different lipid composition and cholesterol fraction in the membrane of healthy and cancer cells [19] are probably the reasons why cancer cells are more vulnerable to plasma treatment. Another theory suggests that plasma species are able to attenuate the antioxidant system of cancer cells [20]. Plasma oxidation of amino acids in proteins, especially oxidation of the thiol groups of Cys residues, can disturb the normal function of some antioxidant enzymes [21]. Indeed, the ROS-induced protein modifications can alter the protein structure and disrupt their function [22]. In particular, a recent study on CAP oxidation of the human epidermal growth factor demonstrated that oxidation leads to a change in structural conformation of this protein, and in its binding affinity with the receptor [23].

In the present study, we will take another step towards the understanding of the selective anti-cancer capacity of plasma, based on the transmembrane protein xC^- antiporter. The xC^- antiporter is responsible for translocation of cystine (CYC, i.e., the negatively oxidized dimeric form of Cys [24]) from the extracellular milieu to inside the cell, and for sending out glutamate (Glu) from the intracellular fluid to outside the cell [25]. Inside the cell, CYC is rapidly modified to Cys that takes part in some synthesis reactions, especially in glutathione biosynthesis. Glutathione is a tripeptide thiol, consisting of Glu, Cys and Gly, which plays an important role in protecting cells against intracellular oxidative stress [25]. The xC^- antiporter is more essential for cancer cells than for healthy cells, as some cancer cells are unable to synthesize intracellular Cys [26]. For instance, lymphoma and leukemia cells do not have any endogenous Cys-synthetic ability, and hence, the CYC uptake from the extracellular milieu by xC^- antiporters is important for their viability. Thus, inhibition of this antiporter in cancer

* Corresponding author. Physics Department, Shahid Beheshti University, G.C., Evin, Tehran, 19839, Iran.
E-mail addresses: Mar_ghasemi@sbu.ac.ir, Maryam.Ghasemitarei@uantwerpen.be (M. Ghasemitarei).

https://doi.org/10.1016/j.abb.2019.108114
Received 25 June 2019; Received in revised form 19 September 2019; Accepted 22 September 2019
Available online 23 September 2019
0003-9861/

cells may lead to Cys starvation, and thus to a decrease of the intracellular glutathione concentration. The depletion of intracellular glutathione levels can subsequently inhibit the cell growth, thereby inducing apoptosis and reducing cancer cell drug resistance [25].

Another difference between healthy and cancer cells is related to their extracellular pH environment. Cancer cells are able to upregulate anaerobic glycolysis, even in the presence of oxygen. Glycolysis is the pathway that converts glucose to pyruvate, which is useful to supply free energy to form high energy molecules, i.e., adenosine triphosphate (ATP) and nicotinamide adenine dinucleotide bonded by a hydrogen atom (NADH). The anaerobic glycolysis stimulates the conversion of pyruvate to lactic acid [27]. To avoid acid-induced apoptosis, some transporters on the membrane of cancer cells export the accumulating acid (i.e., lactic acid) to the extracellular environment [28]. Hence, the extracellular pH in cancer cells becomes acidic. This acidic environment in cancer cells reduces the CYC uptake [29,30]. In this regard, it is interesting to know how plasma, through oxidizing the extracellular amino acid residues of xC^- antiporter, influences the CYC uptake.

Because of the importance of CYC in cancer cell viability, the upregulation of xC^- antiporter has been demonstrated in some cancer cells, such as lymphomas, gliomas and pancreatic cancer cells [31,32]. The main functional subunit of the xC^- protein is xCT (i.e., the so-called light subunit) that is responsible for bidirectional transport of CYC and Glu [25]. The heavy subunit of xC^- antiporter (i.e., 4F2hc) is responsible for holding the antiporter in the membrane. Fig. 1 schematically illustrates the light and heavy subunits of xC^- antiporter. During the counter-transport (i.e., the import of CYC and export of Glu), the xCT subunit of xC^- antiporter can have three conformations, i.e., outward facing (OF), occluded (OCC) and inward facing (IF), the structures of which were modeled recently, and more information about their functions is given in Ref. [33].

One of the important amino acids of the xCT subunit is Cys_{327}, which is not highly conserved, i.e., it is a main target for modification (e.g., mutation or oxidation). Experiments demonstrated that the mutation of this amino acid to Ala, Ser and Thr slightly reduces, whereas mutation to Leu even suppresses the transport function of xC^- antiporter [34]. Cys_{327} is highly reactive and located in the vicinity of the extracellular milieu, the protein channel and the substrate binding site in the OF state of the xCT subunit [34]. Thus, it is conceivable that during plasma treatment, this residue can be oxidized by plasma-generated species. The oxidative modification of Cys_{327}, on the other hand, can also alter the channel conformation and hence the CYC uptake. In addition, Cys can be oxidized in different pathways at different pH conditions. Generally, the thiol group of Cys is easily oxidized by ROS and RNS [35]. In fact, because of the intracellular ROS, especially hydrogen peroxide (H_2O_2), 5% of the Cys residues of cellular proteins are oxidized to sulfunic or cysteic acid [36]. The oxidation pathways of Cys are related to the structure of the oxidant and the reaction conditions

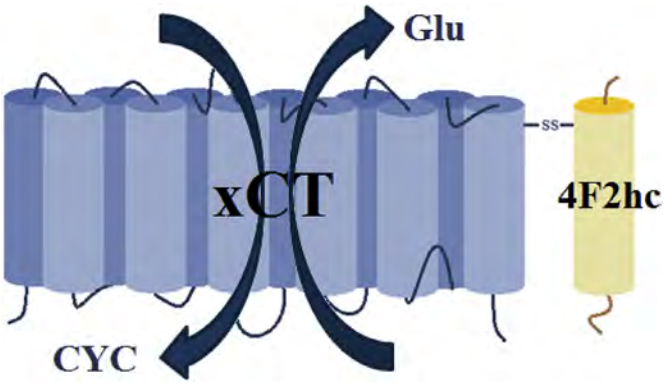

Fig. 1. Schematic representation of the light (xCT) and heavy (4F2hc) subunits of xC^- antiporter.

[37], such as pH. Previous studies showed that in basic pH and in the presence of H_2O_2, Cys is oxidized to Cys sulfonic acid [37,38]. In acidic pH, and in the presence of hydroxyl radical (OH°), H_2O_2 and superoxide (O_2^-), which are all generated by CAP, Cys is oxidized to cysteic acid [38]. These two kinds of oxidation are biologically irreversible reactions, while oxidation of Cys to CYC in neutral pH is a completely reversible reaction.

Based on these considerations, in this study, we investigate the effect of Cys_{327} oxidation to cysteic acid on the transport of CYC across native and oxidized xCT, by applying umbrella sampling (US) simulations. For this purpose, we use the OF conformation of the xCT subunit, which is the first conformation of the xCT subunit (see above); thus, it has access to the extracellular milieu and is completely closed from the intracellular fluid.

2. Computational details

2.1. Model systems

The model system of the native OF conformation is composed of the OF protein embedded in a fully-hydrated palmitoyl-oleoyl-phosphatidylcholine (POPC) bilayer. This system was used in our previous study and a detailed explanation of its preparation is given there [33] as well as in the Supplementary Information. Briefly, the protein sequence (FASTA) of the human xCT [39] subunit was extracted from the NCBI website (https://www.ncbi.nlm.nih.gov/). To construct the OF conformation of xCT, the OF open face of AdiC (PDB ID: 3OB6 [40]) antiporter with similarity 24.83% was chosen as a template, applying the SWISS-MODEL server [41], since the 3D structure of this system was not available in the protein data bank. Subsequently, the OF protein was incorporated into the fully-hydrated POPC lipid bilayer, applying the CHARMM GUI web server [42,43]. The orientation of the model protein into the lipid bilayer surrounding it was determined by the OPM [44] database (http://opm.phar.umich.edu/). To build the oxidized OF system, we modified Cys_{327} of the native OF protein to cysteic acid (CYO_{327}), applying the GaussView software version 5.0.8 [45].

2.2. Molecular dynamics simulation protocols

Molecular dynamics (MD) simulations were carried out using the GROMACS 5.0.4 package [46,47]. Both the native and oxidized OF systems were prepared as follows. The systems were initially energy minimized, applying the steepest descent algorithm. Subsequently, they were equilibrated for 500 ns in the isothermal-isobaric (NPT) ensemble at 310 K and 1 atm. These simulations were repeated three times by changing the values of the initial velocities of the atoms in the system in order to ensure that all three structures of each system are consistent. The Nose-Hoover thermostat [48] in combination with a coupling constant of 1 ps and the semi-isotropic Parrinello-Rahman barostat [49] with a compressibility of $4.5 \times 10^{-5}\,bar^{-1}$ and a coupling constant of 5 ps were applied to equilibrate the systems. The cut-off distance of both the electrostatic and van der Waals interactions was chosen as 12 Å. Electrostatic interactions were treated by the particle mesh Ewald method [50,51] and long-range dispersion corrections were applied for both energy and pressure. The net positive charges of both systems were neutralized by adding chloride ions. Overall, both systems were composed of 202 POPC lipids, the native or oxidized OF protein and 15000 water molecules covering them from top (extracellular part) and bottom (intracellular part), see Supplementary Fig. S2. Both systems were simulated under periodic boundary conditions and the dimension of these systems was $\approx 105 \times 105 \times 95$ Å^3. A time step of 2 fs was used in all simulations, and the CHARMM36 m force field was applied to describe the interatomic interactions in the systems in combination with the TIP3P water model [52]. The CHARMM-type force field parameters for CYC and cysteic acid (i.e., CYO_{327} residue, see above) of the oxidized OF system were derived as follows. Similar to the methods

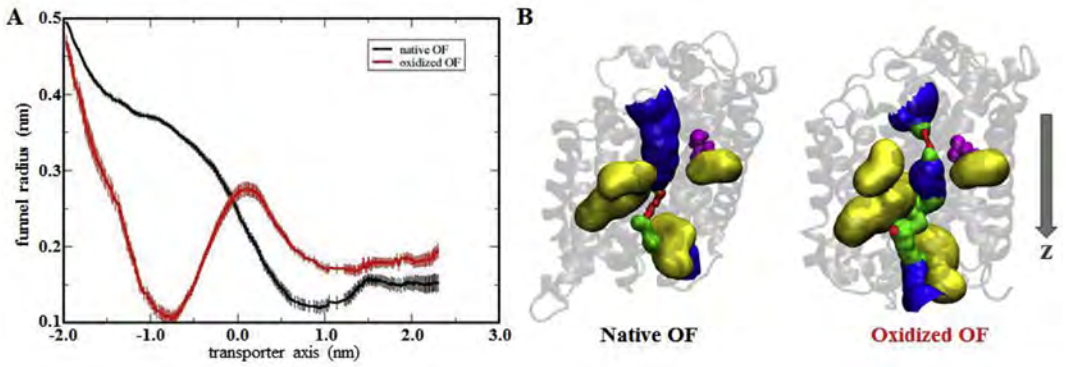

Fig. 2. (A) Profiles of the funnel radii of the native (black) and oxidized (red) OF structures along the main axis (z direction), averaged over the 60 different profiles for each system. (B) Illustration of the changing size (pore radius) of the channels for native (left) and oxidized (right) OF structures, as well as the position of Cys_{327} (left) and CYO_{327} (right) relative to the protein channel (magenta color). Red color indicates that the pore radius is too tight for a water molecule, whereas green shows that there is room for a single water molecule, and blue is used where the radius is double the minimum for a single water molecule. The residues involved in the substrate binding site are illustrated in yellow color. The rest of the protein is shown in light gray Newcartoon view. (For interpretation of the references to color in this figure legend, the reader is referred to the Web version of this article.)

applied by Spoel et al. [53], to obtain the force field parameters of CYC and CYO_{327}, the Gaussian 16 software [54] and the CHARMM general force field (CGenFF) program [55] were implemented. Specifically, to optimize the structures and compute the partial charges, the Gaussian software was used by applying DFT calculations, including the B3LYP functional with standard 6-311G* basis set. It should be noted that according to literature, cysteic acids are formed in proteins as a result of ROS or RNS interactions, and they mostly contain negative charges [36]. Therefore, we also used the negatively charged CYO_{327} in our simulations. The CGenFF program was applied to obtain the parameters for bonds, angles and dihedrals. Finally, the parameters were again renewed by adding the Gaussian-made partial charges to CGenFF-made parameters. The details of the partial charges of the residues in acidic pH of the oxidized OF system are presented in the Supplementary Information. The funnel radius analysis and the US simulations (see below) were applied after equilibration of both systems for 500 ns Note that this equilibration time was sufficient, as the calculated root mean squared deviations (RMSDs) of both the native and oxidized OF systems showed a convergence after 400 ns (see Supplementary Fig. S3). The non-bonded (i.e., Coulomb + van der Waals) interaction energies between some amino acid residues of both systems were computed using the *gmx energy* tool of GROMACS.

2.3. Calculation of the funnel radii

We applied the HOLE program [56] to calculate the profiles of the funnel radii across the channels of both the native and oxidized OF systems. This program is useful to visualize and analyze the pore dimension of protein structures, such as ion channels and transporters. It computes the largest radius of protein channels along the channel vector (i.e., z direction in our case), without overlapping with the van der Waals surface of any atoms. Around 60 configurations were extracted from the last 50 ns of the equilibration simulations (see above) to obtain the average funnel radii along the z direction (i.e., transporter axis) for both native and oxidized OF systems.

2.4. Umbrella sampling (US) simulations

To compute the potentials of mean force (i.e., free energy profiles (FEPs)) of CYC translocation across both the native and oxidized OF systems, the US method was employed. In both structures, the initial position of CYC was chosen in the extracellular milieu, i.e., at −3.9 nm distance from the center of mass (COM) of the protein (i.e., in the z position close to the aperture of the protein channel). CYC was then pulled against the COM of both systems along the z direction with a harmonic biasing force constant of 1000 $kJ.mol^{-1}. nm^{-2}$ and pulling rate of 0.01 $nm.ps^{-1}$. After pulling CYC for 1100 ps, 98 windows (i.e., 49 for the native and 49 for the oxidized system), separated by a distance of ≤ 0.1 nm, were extracted for the US simulations for both the native and oxidized structures. In this manner, the sampling windows spanned the whole protein channel, starting from the extracellular milieu and ending at the end of the protein channel, where the channel is closed from the intracellular milieu. Subsequently, the US simulations were run for 20 ns and the last 15 ns of the trajectory was used to obtain the FEPs. To construct the FEPs the periodic version of the weighted histogram analysis method (WHAM) [57] was applied. Errors associated with the sampling were computed by the bootstrapping method. At last, the final FEP of each system was obtained by averaging over four independently calculated FEPs. These FEPs were calculated using four configurations (for each system) derived from the last 50 ns (i.e., taken at 470, 480, 490 and 500 ns) of the equilibration simulations. In total, 98 × 4 = 392 US simulations were performed to obtain the FEPs for each system.

3. Results and discussion

3.1. Funnel radii analysis

Fig. 2A compares the profiles of the averaged funnel radii, i.e., the largest radii of the pore channels without overlapping with the van der Waals surface of any atom, of the native and oxidized OF systems along the z direction (i.e., across their channels). It is clear that the channel of the native OF system is fully open for CYC passage to the substrate binding site (z ≈ −0.5–0.5 nm), while it is completely closed in the oxidized OF structure, preventing the CYC access to the substrate binding site. The latter can be seen by looking at the funnel radius for the negative values on the transporter axis, which drops to 0.1 nm around −0.8 nm of the protein channel, which is too small for CYC to pass, while the funnel radius of the native OF system is large enough (i.e. ~0.37 nm) in this region. The closure of the pore in the oxidized OF system blocks the access of CYC to the substrate binding site. Therefore, the extracellular CYC is not able to translocate towards the xCT substrate binding site (see also the US results below).

Fig. 2B illustrates the protein channel of the native and oxidized OF systems, and how its size varies along the z direction, which is shown in different colors (i.e., red, green and blue). The red color corresponds to very tight parts of the channels (i.e., channel radius below 0.115 nm), where even a single water molecule cannot permeate (i.e., the passage of CYC is totally blocked). The parts with green color indicate that the channels have enough space for passage of a single water molecule, but

CYC still cannot translocate (i.e., channel radius between 0.115 and 0.230 nm). Hence, only in the blue parts of the channels (i.e., radius above 0.230 nm) the passage of CYC is possible. It is obvious from Fig. 2B that the substrate binding site is not accessible from the extracellular milieu in the oxidized OF system, whereas it is fully accessible in the native OF system. The substrate binding site consists of residues that form temporary bonds with the substrate (i.e., CYC) and play an important role in guiding the substrate into the protein channel. The binding sites on proteins are critical parts of signal transduction pathways [58]. In our previous study we found that Arg_{135}, Arg_{396}, Arg_{126}, Lys_{198} and Arg_{340} are the most important residues in the substrate binding site of the OF state of the xCT subunit, as they strongly bind to CYC [33]. These amino acids are illustrated in Fig. 2B by the yellow color, and they are accessible to CYC only from the protein channel. Therefore, if the channel becomes closed, they will not be accessible for CYC from the extracellular milieu. This is due to oxidation of Cys_{327} to CYO_{327} that leads to conformational changes in the channel, thereby affecting the CYC permeation (see next section).

3.2. Conformations of the native and oxidized of structures

We found from previous section that the channel of the oxidized OF system is completely closed from the extracellular milieu, which is the result of Cys_{327} oxidation to CYO_{327}. Monitoring of the amino acids around the closed part showed that the rearrangements in the side chains of Tyr_{244} and CYO_{327} residues have a critical role in closure of the OF channel. Fig. 3 shows the positions of Tyr_{244} and Cys_{327} (Fig. 3A), as well as Tyr_{244} and CYO_{327} (Fig. 3B) of the native and oxidized OF channels, respectively. The comparison of Fig. 3A and B clearly shows that the rotation of the Tyr_{244} side chain and the change in orientation of the CYO_{327} side chain towards Tyr_{244} leads to a closure of the channel. Indeed, the calculated distance between the alcohol group of Tyr_{244} and the sulfur atom of CYO_{327}, (i.e., ~8.2 Å, see Table 1) was found to be shorter than that between the alcohol group of Tyr_{244} and the sulfur atom of Cys_{327} (i.e., ~15.5 Å, see Table 1), resulting in a narrowing of the channel after oxidation took place.

Krammer et al. [59] determined that the rotameric state of Trp_{202} in the AdiC transporter structure was crucial for occlusion of the OF to OCC state. Their study stressed that the OF state of the AdiC conformation without proper rotation of the Trp_{202} side chain cannot occlude completely. This amino acid is equivalent to Tyr_{244} in the xCT subunit (i.e., at the same position as Tyr_{244} in the amino acid sequence). Thus, we believe that Tyr_{244} plays an important role in channel closure, which was the case in our study.

Table 1 illustrates the averaged distance between the backbones (i.e., alpha carbons) and side chains of Tyr_{244} and Cys_{327} for the native OF state and of Tyr_{244} and CYO_{327} for the oxidized OF state of the xCT subunit.

It is obvious that after oxidation of Cys_{327} to CYO_{327} the overall distance between these residues and Tyr_{244} decreases, which is most clear for S–OH (i.e., drop by about a factor two). This again indicates that Cys_{327} oxidation in the OF structure leads to conformational changes in the channel, resulting in closure of this channel and hence blockage of the CYC uptake.

Table 1
Averaged distance between the backbones (i.e., C_α-C_α) and sidechains (i.e., S–OH) of Cys_{327} and Tyr_{244} in the native OF state and of CYO_{327} and Tyr_{244} in the oxidized OF proteins.

residues	C_α-C_α (Å)	S–OH (Å)
Cys_{327}-Tyr_{244} (native OF)	19.04 ± 0.03	15.47 ± 0.04
CYO_{327}-Tyr_{244} (oxidized OF)	14.44 ± 0.02	8.15 ± 0.02

Table 2
Non-bonded (i.e., Coulomb + van der Waals) interaction energies calculated for Cys_{327}, CYO_{327} and Tyr_{244} of the native and oxidized OF systems, with each other and with the rest of the system. Note that the interaction energies between Cys_{327}-Tyr_{244} and CYO_{327}-Tyr_{244} correspond to the native and oxidized OF structures, respectively. The same applies to Cys_{327}-rest of the system and CYO_{327}-rest of the system.

protein	Cys_{327}/CYO_{327}-Tyr_{244} (kJ/mol)	Cys_{327}/CYO_{327}-rest (kJ/mol)	Tyr_{244}-rest (kJ/mol)
native OF	≈ 0	− 5.1 ± 0.7	− 82.2 ± 2.0
oxidized OF	≈ 0	− 160.0 ± 6.2	− 100.6 ± 1.3

3.3. Analysis of the interaction energies

Table 2 illustrates the non-bonded (i.e., Coulomb + van der Waals) interaction energies between Cys_{327}-Tyr_{244}, Cys_{327}-rest of the system and Tyr_{244}-rest of the system in the native OF system, as well as between CYO_{327}-Tyr_{244}, CYO_{327}-rest of the system and Tyr_{244}-rest of the system in the oxidized OF system.

It is obvious that after oxidation of Cys_{327} to cysteic acid (CYO_{327}), the interaction energy becomes more negative (i.e., stronger interaction) in all cases, although the change in energy for CYO_{327}-Tyr_{244} (second column in Table 2) was not significant. The latter is probably because the distance between CYO_{327} and Tyr_{244} is still relatively long (~8.2 Å; see Fig. 3B and Table 1), which is not enough to make a H-bond, although this H-bond interaction for the S–H system is inherently weaker [60]. On the other hand, the interaction energy between CYO_{327} and the rest of the system, attributed to the attractive (namely, Coulomb) interaction of three oxygen atoms in the side chain of CYO_{327} with the surrounding amino acids, was much stronger than the energy between Cys_{327} and the rest of system (third column). In general, the movement and rotation of the side chain of Tyr_{244} and a change in the orientation of the side chain of CYO_{327} results in a rearrangement of the

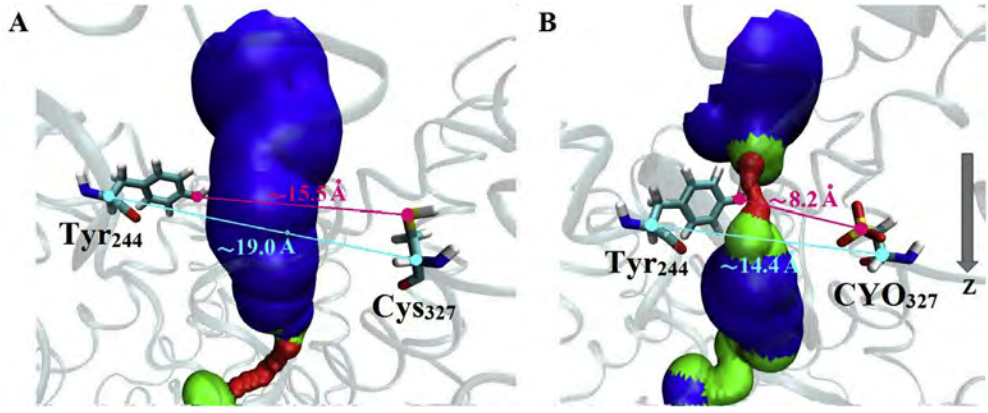

Fig. 3. Orientations of Tyr_{244} and Cys_{327} (A) and Tyr_{244} and CYO_{327} (B) in the channels of the native (A) and oxidized (B) OF proteins, indicating the distance between the alcohol group of Tyr_{244} and the sulfur atom of Cys_{327} (~15.5 Å) (A), and between the alcohol group of Tyr_{244} and the sulfur atom of CYO_{327} (~8.2 Å) (B), and hence the narrowing of the channel upon oxidation.

surrounding amino acids, bringing Tyr_{244} and CYO_{327} in the vicinity of some new amino acids, allowing to make H-bonds with some of them. These mediator amino acids are Ala_{60}, Gly_{61}, Ala_{145}, Phe_{146} and Lys_{198}, resulting in H-bonds with all of them, while they did not have any H-bonds with Cys_{327} and Tyr_{244} prior to Cys_{327} oxidation. Moreover, some other amino acids, such as Phe_{63}, Ile_{64}, Thr_{139}, Arg_{148}, Tyr_{149}, Ser_{330} and Met_{331}, make H-bonds with both CYO_{327} and Tyr_{244}, while they had H-bonds with only the backbone of Cys_{327} before oxidation. Specifically, among all mentioned amino acids, Ala_{60}, Gly_{61} are found to be the most important ones because of two reasons. Firstly, they are in the vicinity of the closed parts of the protein channel (cf. red color part in Fig. 3B). Secondly, they did not have any H-bonds with Cys_{327} and Tyr_{244} before oxidation. The positions of Ala_{60} and Gly_{61} relative to the channels of both the native and oxidized OF proteins are illustrated in the Supplementary Fig. S4. Moreover, the distances between these two amino acids and other residues are given in Table S2, together with the explanation about their interactions (see the Supplementary Information). It is important to mention that the distance of Ala_{60} and Gly_{61} with CYO_{327} partially increased, whereas their distances with Tyr_{244} decreased noticeably. In general, in the oxidized OF system, these four amino acids (Ala_{60}, Gly_{61}, CYO_{327} and Tyr_{244}) moved toward each other, making the channel more narrow, eventually blocking the protein channel in this area.

We further performed a detailed analysis of the conformational changes together with these important amino acids, by aligning the native and oxidized structures of (see Supplementary Figs. S5 and S6 and explanations therein). Specifically, we studied the positions of the transmembrane (TM) domains (i.e., TM1, TM3, TM5, TM6 and TM8), which contain the above mentioned amino acids. In general, we found that among the TM domains, TM1, TM5 and TM6 moved towards TM8, which resulted in a change of the channel size. This subsequently led to a dramatic increase of the interaction energy between CYO_{327} and other amino acids (including Ala_{60}, Gly_{61} and Tyr_{244}) surrounding this residue. This is summarized in Fig. 4, illustrating the positions of four important amino acids (i.e., Cys_{327}/CYO_{327}, Tyr_{244}, Ala_{60} and Gly_{61}) by superimposing the structures of the native and oxidized OF systems. Hence, we can conclude that the reorientation of these amino acids, and thereby the movement of the TM domains to which they belong, led to a narrowing of the channel after oxidation (cf. also Figs. 2 and 3), resulting in a blocking of the access of CYC to the substrate binding site of the OF system.

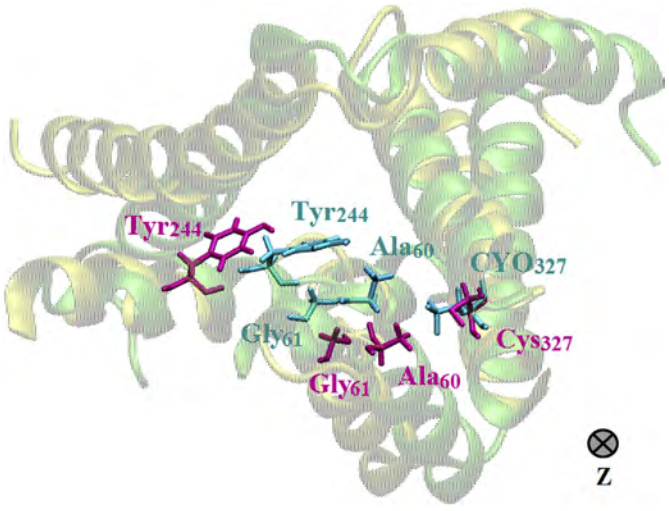

Fig. 4. Superimposed structures of the native (yellow) and oxidized (green) OF from top view, together with some important amino acids (i.e., Cys_{327}/CYO_{327}, Tyr_{244}, Ala_{60} and Gly_{61}) depicted in magenta (native system) and cyan (oxidized system) colors. (For interpretation of the references to color in this figure legend, the reader is referred to the Web version of this article.)

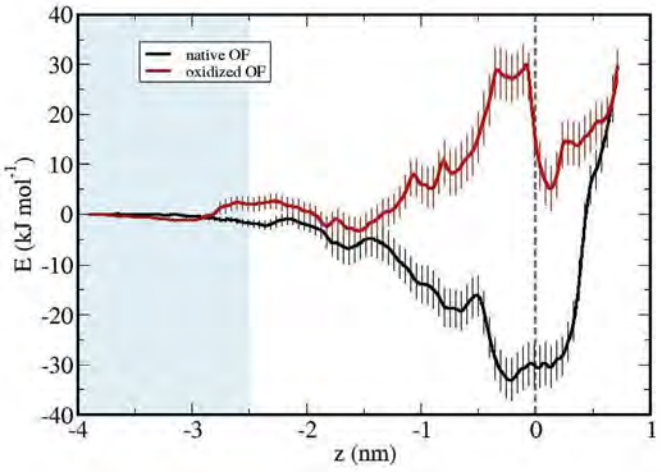

Fig. 5. Free energy profiles for the translocation of CYC across the native and oxidized OF structures. The position of the center of mass (COM) is indicated by the gray dashed line. The light blue color corresponds to the extracellular water phase. (For interpretation of the references to color in this figure legend, the reader is referred to the Web version of this article.)

3.4. Free energy profiles (FEPs)

The FEPs of CYC translocation across the channels of both the native and oxidized OF systems are compared in Fig. 5.

It is clear that oxidation of Cys_{327} to CYO_{327} and thus the reorientation of this and other residues around the substrate binding site, including Tyr_{244}, creates a free energy barrier of 33.9 $kJmol^{-1}$ for CYC translocation, making the CYC penetration to the substrate binding site more difficult than in the native OF state. In our previous study we found that the free energy barrier of CYC translocation through the modified OF state (i.e., Cys_{327} modification to Ala_{327}) was 32.4 $kJmol^{-1}$. Hence, the barrier becomes even higher in the oxidized OF system. Our results thus indicate that oxidation of Cys_{327} to CYO_{327}, which can be caused by cold atmospheric plasma (CAP), is more effective than mutation of this amino acid to Ala in inhibition of the xC^- antiporter.

4. Conclusions

We investigated the effects of Cys_{327} oxidation in acidic pH on CYC translocation across the OF conformation of the xCT subunit of the xC^- antiporter, which might be important as a future cancer therapy target by using CAP. Indeed, in cancer cells an enhanced transport of CYC across the xC^- antiporter is observed, and this protects the cancer cells from intracellular oxidative stress. If the CYC uptake is inhibited by oxidation of some amino acid residues of the xCT subunit via CAP, this can reduce the cellular protection from oxidative stress, as well as reduce cancer cell drug resistance, eventually leading to cancer cell death.

We applied US simulations to study the permeation of CYC across the native and oxidized OF systems, based on Cys_{327} oxidation to cysteic acid (CYO_{327}). The free energy profiles of CYC translocation across the native and oxidized OF structures showed that oxidation of Cys_{327} to CYO_{327} makes the CYC transportation more difficult, creating a barrier of 33.9 $kJmol^{-1}$, thereby leading to a decrease in the CYC permeation rate. Comparison of the funnel radii profiles of both the native and oxidized OF states showed that oxidation leads to closure of the protein channel from the extracellular milieu, so that the substrate binding site is not accessible anymore from outside of the cell. By monitoring the amino acids around the closed part of the oxidized OF state, we found that oxidation results in a rearrangement of the amino acids around the oxidized Cys_{327} in the protein channel. Among these amino acids, Tyr_{244} is the most effective one on closure of the protein channel. This amino acid becomes closer to CYO_{327} by rotating its side

chain, whereas CYO_{327} also changes its orientation towards Tyr_{244}, together making the channel narrower. These rearrangements of the amino acid residues form H-bonds with some neighboring amino acids, such as Ala_{60} and Gly_{61}.

This study is important, since it elucidates the effect of oxidation of Cys_{327} on closure of the protein channel, thereby making CYC uptake by the xCT subunit of the xC^- antiporter more difficult. This oxidation can happen as a result of e.g., CAP application to cancer cells at acidic pH. Hence, this study might explain the possible mechanism of CYC starvation in cancer cells, through inhibition of the xC^- antiporter, which results in a depletion of the intracellular level of glutathione, and consequently, in inhibition of cell growth, inducing apoptosis and reducing the cancer cell drug resistance.

Acknowledgements

M. G. acknowledges funding from the Ministry of Science, Research and Technology of Iran and from the University of Antwerp in Belgium. M. Y. gratefully acknowledges financial support from the Research Foundation − Flanders (FWO), grant number 1200219N. The computational work was carried out using the Turing HPC infrastructure at the CalcUA core facility of the Universiteit Antwerpen (UA), a division of the Flemish Supercomputer Center VSC, funded by the Hercules Foundation, the Flemish Government (department EWI) and the UA.

Finally, we thank A. S. Mashayekh Esfehan and A. Mohseni for their important comments on the manuscript.

Appendix A. Supplementary data

Supplementary data to this article can be found online at https://doi.org/10.1016/j.abb.2019.108114.

References

[1] M.G. Kong, G. Kroesen, G. Morfill, T. Nosenko, T. Shimizu, J. van Dijk, J.L. Zimmermann, Plasma medicine: an introductory review, New J. Phys. 11 (11) (2009) 115012.
[2] R. Ranjan, P. Krishnamraju, T. Shankar, S. Gowd, Nonthermal plasma in dentistry: an update, J. Int. Soc. Prev. Community Dent. 7 (3) (2017) 71.
[3] G. Fridman, M. Peddinghaus, M. Balasubramanian, H. Ayan, A. Fridman, A. Gutsol, A. Brooks, Blood coagulation and living tissue sterilization by floating-electrode dielectric barrier discharge in air, Plasma Chem. Plasma Process. 26 (4) (2006) 425–442.
[4] M. Keidar, A. Shashurin, O. Volotskova, M. Ann Stepp, P. Srinivasan, A. Sandler, B. Trink, Cold atmospheric plasma in cancer therapy, Phys. Plasmas 20 (5) (2013) 057101.
[5] S. Fathollah, S. Mirpour, P. Mansouri, A.R. Dehpour, M. Ghoranneviss, N. Rahimi, Z.S. Naraghi, R. Chalangari, K.M. Chalangari, Investigation on the effects of the atmospheric pressure plasma on wound healing in diabetic rats, Sci. Rep. 6 (2016) 19144.
[6] E.A. Ratovitski, X. Cheng, D. Yan, J.H. Sherman, J. Canady, B. Trink, M. Keidar, Anti-cancer therapies of 21st century: novel approach to treat human cancers using cold atmospheric plasma, Plasma Process. Polym. 11 (12) (2014) 1128–1137.
[7] G. Fridman, A. Shereshevsky, M.M. Jost, A.D. Brooks, A. Fridman, A. Gutsol, V. Vasilets, G. Friedman, Floating electrode dielectric barrier discharge plasma in air promoting apoptotic behavior in melanoma skin cancer cell lines, Plasma Chem. Plasma Process. 27 (2) (2007) 163–176.
[8] M. Laroussi, From killing bacteria to destroying cancer cells: 20 years of plasma medicine, Plasma Process. Polym. 11 (12) (2014) 1138–1141.
[9] S. Mashayekh, H. Rajaee, M. Akhlaghi, B. Shokri, Z.M. Hassan, Atmospheric-pressure plasma jet characterization and applications on melanoma cancer treatment (B/16-F10), Phys. Plasmas 22 (9) (2015) 093508.
[10] X. Yan, Z. Xiong, F. Zou, S. Zhao, X. Lu, G. Yang, G. He, K. Ostrikov, Plasma-induced death of HepG2 cancer cells: intracellular effects of reactive species, Plasma Process. Polym. 9 (1) (2012) 59–66.
[11] H. Lee, C. Shon, Y. Kim, S. Kim, G. Kim, M.G. Kong, Degradation of adhesion molecules of G361 melanoma cells by a non-thermal atmospheric pressure microplasma, New J. Phys. 11 (11) (2009) 115026.
[12] X. Cheng, W. Murphy, N. Recek, D. Yan, U. Cvelbar, A. Vesel, M. Mozetič, J. Canady, M. Keidar, J.H. Sherman, Synergistic effect of gold nanoparticles and cold plasma on glioblastoma cancer therapy, J. Phys. D Appl. Phys. 47 (33) (2014) 335402.
[13] N. Barekzi, M. Laroussi, Dose-dependent killing of leukemia cells by low-temperature plasma, J. Phys. D Appl. Phys. 45 (42) (2012) 422002.
[14] G.-Y. Liou, P. Storz, Reactive oxygen species in cancer, Free Radic. Res. 44 (5) (2010) 479–496.
[15] M. Keidar, R. Walk, A. Shashurin, P. Srinivasan, A. Sandler, S. Dasgupta, R. Ravi, R. Guerrero-Preston, B. Trink, Cold plasma selectivity and the possibility of a paradigm shift in cancer therapy, Br. J. Canc. 105 (9) (2011) 1295.
[16] R.A. Cairns, I.S. Harris, T.W. Mak, Regulation of cancer cell metabolism, Nat. Rev. Cancer 11 (2011) 85.
[17] D. Yan, A. Talbot, N. Nourmohammadi, J.H. Sherman, X. Cheng, M. Keidar, Toward understanding the selective anticancer capacity of cold atmospheric plasma—a model based on aquaporins, Biointerphases 10 (4) (2015) 040801.
[18] D. Yan, H. Xiao, W. Zhu, N. Nourmohammadi, L.G. Zhang, K. Bian, M. Keidar, The role of aquaporins in the anti-glioblastoma capacity of the cold plasma-stimulated medium, J. Phys. D Appl. Phys. 50 (5) (2017) 055401.
[19] J. Van der Paal, E.C. Neyts, C.C. Verlackt, A. Bogaerts, Effect of lipid peroxidation on membrane permeability of cancer and normal cells subjected to oxidative stress, Chem. Sci. 7 (1) (2016) 489–498.
[20] S. Zhao, Z. Xiong, X. Mao, D. Meng, Q. Lei, Y. Li, P. Deng, M. Chen, M. Tu, X. Lu, Atmospheric pressure room temperature plasma jets facilitate oxidative and nitrative stress and lead to endoplasmic reticulum stress dependent apoptosis in HepG2 cells, PLoS One 8 (8) (2013) e73665.
[21] D. Yan, A. Talbot, N. Nourmohammadi, X. Cheng, J. Canady, J. Sherman, M. Keidar, Principles of using cold atmospheric plasma stimulated media for cancer treatment, Sci. Rep. 5 (2015) 18339.
[22] E. Cabiscol, J. Ros, Oxidative Damage to Proteins: Structural Modifications and Consequences in Cell Function, Redox Proteomics: from Protein Modification to Cellular Dysfunction and Disease, (2006), pp. 399–471.
[23] M. Yusupov, J.W. Lackmann, J. Razzokov, S. Kumar, K. Stapelmann, A. Bogaerts, Impact of plasma oxidation on structural features of human epidermal growth factor, Plasma Process. Polym. 15 (8) (2018) 1800022.
[24] S. Bannai, E. Kitamura, Role of proton dissociation in the transport of cystine and glutamate in human diploid fibroblasts in culture, J. Biol. Chem. 256 (11) (1981) 5770–5772.
[25] M. Lo, Y.Z. Wang, P.W. Gout, The x cystine/glutamate antiporter: a potential target for therapy of cancer and other diseases, J. Cell. Physiol. 215 (3) (2008) 593–602.
[26] P. Gout, Y. Kang, D. Buckley, N. Bruchovsky, A. Buckley, Increased cystine uptake capability associated with malignant progression of Nb2 lymphoma cells, Leukemia 11 (8) (1997) 1329.
[27] R.A. Gatenby, R.J. Gillies, Why do cancers have high aerobic glycolysis? Nat. Rev. Cancer 4 (11) (2004) 891.
[28] H. Izumi, T. Torigoe, H. Ishiguchi, H. Uramoto, Y. Yoshida, M. Tanabe, T. Ise, T. Murakami, T. Yoshida, M. Nomoto, Cellular pH regulators: potentially promising molecular targets for cancer chemotherapy, Cancer Treat Rev. 29 (6) (2003) 541–549.
[29] J. Lewerenz, R. Dargusch, P. Maher, Lactacidosis modulates glutathione metabolism and oxidative glutamate toxicity, J. Neurochem. 113 (2) (2010) 502–514.
[30] M. Bassi, E. Gasol, M. Manzoni, M. Pineda, M. Riboni, R. Martín, A. Zorzano, G. Borsani, M. Palacín, Identification and characterisation of human xCT that co-expresses, with 4F2 heavy chain, the amino acid transport activity system xc–, Pflüg. Arch. 442 (2) (2001) 286–296.
[31] M. Lo, V. Ling, Y. Wang, P. Gout, The x c− cystine/glutamate antiporter: a mediator of pancreatic cancer growth with a role in drug resistance, Br. J. Canc. 99 (3) (2008) 464.
[32] J. Lewerenz, S.J. Hewett, Y. Huang, M. Lambros, P.W. Gout, P.W. Kalivas, A. Massie, I. Smolders, A. Methner, M. Pergande, The cystine/glutamate antiporter system xc− in health and disease: from molecular mechanisms to novel therapeutic opportunities, Antioxidants Redox Signal. 18 (5) (2013) 522–555.
[33] M. Ghasemitarei, M. Yusupov, J. Razzokov, B. Shokri, A. Bogaerts, Transport of cystine across xC− antiporter, Arch. Biochem. Biophys. 664 (2019) 117–126.
[34] M. Jiménez-Vidal, E. Gasol, A. Zorzano, V. Nunes, M. Palacín, J. Chillarón, Thiol modification of cysteine 327 in the eighth transmembrane domain of the light subunit xCT of the heteromeric cystine/glutamate antiporter suggests close proximity to the substrate binding site/permeation pathway, J. Biol. Chem. 279 (12) (2004) 11214–11221.
[35] W. Vogt, Oxidation of methionyl residues in proteins: tools, targets, and reversal, Free Radic. Biol. Med. 18 (1) (1995) 93–105.
[36] B.J. Williams, C.K. Barlow, K.L. Kmiec, W.K. Russell, D.H. Russell, Negative ion fragmentation of cysteic acid containing peptides: cysteic acid as a fixed negative charge, J. Am. Soc. Mass Spectrom. 22 (9) (2011) 1622–1630.
[37] A.R. Katritzky, N.G. Akhmedov, O.V. Denisko, 1H and 13C NMR spectroscopic study of oxidation of d, l-cystine and 3, 3′-dithiobis (propionic acid) with hydrogen peroxide in aqueous solution, Magn. Reson. Chem. 41 (1) (2003) 37–41.
[38] J.W. Purdie, γ radiolysis of cystine in aqueous solution. Dose-rate effects and a proposed mechanism, J. Am. Chem. Soc. 89 (2) (1967) 226–230.
[39] E. Gasol, M. Jiménez-Vidal, J. Chillarón, A. Zorzano, M. Palacín, Membrane topology of system xc-light subunit reveals a re-entrant loop with substrate-restricted accessibility, J. Biol. Chem. 279 (30) (2004) 31228–31236.
[40] L. Kowalczyk, M. Ratera, A. Paladino, P. Bartoccioni, E. Errasti-Murugarren, E. Valencia, G. Portella, S. Bial, A. Zorzano, I. Fita, Molecular basis of substrate-induced permeation by an amino acid antiporter, Proc. Natl. Acad. Sci. 108 (10) (2011) 3935–3940.
[41] A. Waterhouse, M. Bertoni, S. Bienert, G. Studer, G. Tauriello, R. Gumienny, F.T. Heer, T.A.P. de Beer, C. Rempfer, L. Bordoli, SWISS-MODEL: homology modelling of protein structures and complexes, Nucleic Acids Res. 46 (W1) (2018) W296–W303.
[42] S. Jo, T. Kim, V.G. Iyer, W. Im, CHARMM-GUI: a web-based graphical user interface for CHARMM, J. Comput. Chem. 29 (11) (2008) 1859–1865.
[43] E.L. Wu, X. Cheng, S. Jo, H. Rui, K.C. Song, E.M. Dávila-Contreras, Y. Qi, J. Lee,

V. Monje-Galvan, R.M. Venable, J.B. Klauda, W. Im, CHARMM-GUI Membrane Builder toward realistic biological membrane simulations, J. Comput. Chem. 35 (27) (2014) 1997–2004.
[44] M.A. Lomize, I.D. Pogozheva, H. Joo, H.I. Mosberg, A.L. Lomize, OPM database and PPM web server: resources for positioning of proteins in membranes, Nucleic Acids Res. 40 (D1) (2011) D370–D376.
[45] A. Frisch, H.P. Hratchian, R.D. Dennington Ii, T.A. Keith, J. Millam, B. Nielsen, A.J. Holder, J. Hiscocks, GaussView Version 5.0. 8, Gaussian, Inc., Wallingford, CT, 2009.
[46] S. Pronk, S. Páll, R. Schulz, P. Larsson, P. Bjelkmar, R. Apostolov, M.R. Shirts, J.C. Smith, P.M. Kasson, D. Van Der Spoel, Gromacs 4.5: a high-throughput and highly parallel open source molecular simulation toolkit, Bioinformatics 29 (7) (2013) 845–854.
[47] M.J. Abraham, T. Murtola, R. Schulz, S. Páll, J.C. Smith, B. Hess, E. Lindahl, GROMACS: high performance molecular simulations through multi-level parallelism from laptops to supercomputers, SoftwareX 1 (2015) 19–25.
[48] D.J. Evans, B.L. Holian, The nose–hoover thermostat, J. Chem. Phys. 83 (8) (1985) 4069–4074.
[49] M. Parrinello, A. Rahman, Polymorphic transitions in single crystals: a new molecular dynamics method, J. Appl. Phys. 52 (12) (1981) 7182–7190.
[50] T. Darden, D. York, L. Pedersen, Particle mesh Ewald: an N· log (N) method for Ewald sums in large systems, J. Chem. Phys. 98 (12) (1993) 10089–10092.
[51] U. Essmann, L. Perera, M.L. Berkowitz, T. Darden, H. Lee, L.G. Pedersen, A smooth particle mesh Ewald method, J. Chem. Phys. 103 (19) (1995) 8577–8593.
[52] P. Bjelkmar, P. Larsson, M.A. Cuendet, B. Hess, E. Lindahl, Implementation of the CHARMM force field in GROMACS: analysis of protein stability effects from correction maps, virtual interaction sites, and water models, J. Chem. Theory Comput. 6 (2) (2010) 459–466.
[53] D. van der Spoel, P.J. van Maaren, C. Caleman, GROMACS molecule & liquid database, Bioinformatics 28 (5) (2012) 752–753.
[54] R.A. Gaussian09, 1, M.J. Frisch, G.W. Trucks, H.B. Schlegel, G.E. Scuseria, M.A. Robb, J.R. Cheeseman, G. Scalmani, V. Barone, B. Mennucci, G.A. Petersson, et al., 121 Gaussian, Inc., Wallingford CT, 2009, pp. 150–166.
[55] K. Vanommeslaeghe, E. Hatcher, C. Acharya, S. Kundu, S. Zhong, J. Shim, E. Darian, O. Guvench, P. Lopes, I. Vorobyov, CHARMM general force field: a force field for drug-like molecules compatible with the CHARMM all-atom additive biological force fields, J. Comput. Chem. 31 (4) (2010) 671–690.
[56] O.S. Smart, J.G. Neduvelil, X. Wang, B. Wallace, M.S. Sansom, HOLE: a program for the analysis of the pore dimensions of ion channel structural models, J. Mol. Graph. 14 (6) (1996) 354–360.
[57] J.S. Hub, B.L. De Groot, D. Van Der Spoel, g_wham-a free weighted histogram analysis implementation including robust error and autocorrelation estimates, J. Chem. Theory Comput. 6 (12) (2010) 3713–3720.
[58] D. Xu, S.I. Jalal, G.W. Sledge, S.O. Meroueh, Small-molecule binding sites to explore protein–protein interactions in the cancer proteome, Mol. Biosyst. 12 (10) (2016) 3067–3087.
[59] E.-M. Krammer, K. Ghaddar, B. André, M. Prévost, Unveiling the mechanism of arginine transport through AdiC with molecular dynamics simulations: the guiding role of aromatic residues, PLoS One 11 (8) (2016) e0160219.
[60] H.S. Biswal, P.R. Shirhatti, S. Wategaonkar, O− H··· O versus O− H··· S hydrogen bonding I: experimental and computational studies on the p-cresol· H2O and p-cresol· H2S complexes, J. Phys. Chem. A 113 (19) (2009) 5633–5643.